Research Article
DOI: http://dx.doi.org/10.2110/palo.2020.010
METAZOAN REEF CONSTRUCTION IN A MIDDLE ORDOVICIAN SEASCAPE: A CASE STUDY FROM THE MINGAN ARCHIPELAGO, QUEBEC
AMELIA PENNY,[1] ANDRÉ DESROCHERS,[2] and BJÖRN KRÖGER[1]
[1]University of Helsinki, Finnish Museum of Natural History, 00560 Helsinki, Finland
[2]University of Ottawa, STEM Complex, 150 Louis-Pasteur Private, Ottawa, Ontario, Canada
email: amelia.penny@helsinki.fi
ABSTRACT: The Ordovician (485–444 Ma) saw a global shift from microbial- to skeletal-dominated reefs, and the rise of corals and bryozoans as important reef-builders. Hypothetically, increasingly morphologically diverse and abundant reef-building metazoans increased spatial habitat heterogeneity in reef environments, an important component of reefs' capacity to support diverse communities. Quantifying the spatial scale and extent of this heterogeneity requires three-dimensional exposures of well-preserved reefs whose composition and spatial arrangement can be measured. The Darriwilian (c. 467–458 Ma) carbonate sequence of the Mingan Archipelago, Quebec, presents such exposures, and also provides an opportunity to establish how the distribution of skeletal-dominated metazoan reefs contributed to, and was influenced by, seafloor relief. This study includes two transects through a 200–300 m wide paleo-reef belt, which developed along a rocky paleo-coast line. The reefs are typically micrite-rich, meter-scale mounds, locally forming larger complexes. Here, we present quantitative evaluations of the composition of these reefs, and detailed mapping of reef distributions. There is high compositional heterogeneity between reefs at spatial scales ranging from meters to kilometers, contributed by differences in the volumetric contribution of skeletal material to the reef core, and in the identity of the dominant reef-builders. We suggest that the abundance and morphological diversity of Middle Ordovician reef building metazoans made them important contributors to environmental and substrate heterogeneity, likely enhancing the diversity of reef-dwelling communities.
INTRODUCTION
For the first approximately 65 million years of the Phanerozoic, reefs were dominated by micro-organisms, often in association with communities of sponges: archaeocyaths in the early Cambrian, lithistid sponges in the later Cambrian, and lithistid, calathiid, and pulchrilaminid sponges in the Early Ordovician (Rowland and Shapiro 2002; Webby 2002; Lee and Riding 2018). From the Tremadocian onwards, robust skeletal metazoans including tabulate corals, stromatoporoids, and bryozoans became progressively more important reef-builders, often in association with pre-existing lithistid sponge-microbial communities (Pratt and James 1982; Adachi et al. 2012; Li et al. 2017; Lee and Riding 2018). By the Middle Ordovician, a shift from microbial- to skeletal-dominated reef construction had occurred in shallow marine settings, alongside an increase in the diversity of reef-building metazoans (e.g., Adachi et al. 2011, 2013) and an expansion of skeletal-dominated metazoan reefs into previously level-bottom environments (Kröger et al. 2017). Changes in the identity, morphology, diversity, and abundance of reef-building organisms can have major impacts on reef-dwelling communities (Roberts and Ormond 1987; Jones et al. 2004; Alvarez-Filip et al. 2011; Messmer et al. 2011). Several types of ecological interactions mediate these impacts, but they occur in part because reef-builders alter their abiotic environment so as to modify resource flow through their communities, a type of ecological interaction known as ecosystem engineering (Jones et al. 1994). Reef-builders create spatial variation in environmental conditions (habitat heterogeneity) at multiple spatial scales, allowing large numbers of species to coexist, promoting local diversity and speciation (Rocha et al. 2005; Kiessling et al. 2010). While changes to reef-building communities through the Ordovician have been documented in superb detail (e.g., Pratt and James 1982; Adachi et al. 2011, 2012, 2013; Li et al. 2017; Kröger et al.

2017), the impacts of these changes on habitat heterogeneity in shallow marine environments have been largely unexplored. The influence of changes in reef-building on Middle Ordovician seascapes may be of particular importance because it coincides with the ecological changes of the Great Ordovician Biodiversification Event (GOBE) (Stigall et al. 2019).

Middle Ordovician reef-bearing localities with sufficiently extensive exposure to allow two-dimensional spatial mapping of reef composition, and constraints on paleo-relief, are relatively rare. The Mingan Archipelago, Quebec, presents an excellent opportunity for these investigations on a Darriwilian (467.3–458.4 Ma) epeiric carbonate platform. Here, we quantify how metazoan reef-builders contributed heterogeneity and hard substrate to otherwise muddy or sandy marine environments at multiple spatial scales, and investigate the past interactions between local environments and reef-building animals. Detailed documentation of Middle Ordovician reef habitats, together with characterization of their faunas and the impacts of reef-building on the environment, are crucial steps towards understanding the feedbacks between environmental conditions and biodiversity in early Paleozoic shallow marine environments.

GEOLOGICAL SETTING

Stratigraphy of the Mingan Formation

The Mingan Archipelago is a chain of about 30 islands close to the north shore of the Gulf of St. Lawrence (Fig. 1). It contains extensive exposures of Lower–Middle Ordovician strata, including abundant limestones and dolostones (Desrochers 1985) (Fig. 2). Exposures record a succession of almost undeformed shallow-water platform carbonates, showing only a slight southward dip of 1–2˚ and attaining a thickness of ~120 m (Desrochers and James 1988, 1989). The succession unconformably overlies Precambrian (Grenvillian) basement, and is divided into two formations: the lower, dolomitic Romaine Formation and the overlying limestones of the Mingan Formation, separated by the Post-Romaine Paleokarst (Desrochers and James 1989; Desrochers et al. 2012).

The Mingan Formation is late Darriwilian in age, and is a transgressive depositional sequence containing several second-order transgressions and regressions (Desrochers and James 1989). It is divided into the Corbeau, Perroquet, Fantôme, and Grande Pointe members (Desrochers 1985). Widespread metazoan bioherms and bioherm complexes occur in the Grande Pointe Member, and biostromes occur in the Perroquet Member (Figs. 1, 2) (Desrochers and James 1989). The bioherms include some of the first extensive development of bryozoan reefs in North America, and 13 bryozoan species occur in bioherms, biostromes, and inter-reef facies of the Mingan Archipelago (Bolton and Cuffey 2005). Other important metazoan reef-builders include diverse lithistid sponges (Desrochers and James 1989; Rigby and Desrochers 1995), and the tabulate corals *Eofletcheria incerta* and *Billingsaria parva* (Desrochers 1985; Desrochers and James 1989).

The Grande Pointe Member is a limestone unit representing several shallow subtidal paleoenvironments including lagoons, patch reefs, sand shoals, and low-energy, open shelf settings (Desrochers and James 1989). At its base is the intra-Mingan unconformity, which dates to within the late Darriwilian *Cahabgnathus friendvillensis* conodont-zone and represents no more than 1–2 million years of missing record (Dix et al. 2013; McLaughlin et al. 2016) (Fig. 2). The intra-Mingan unconformity has a syndepositional relief of around 20 m, which had a strong influence on facies distribution within the Grande Pointe Member. Skeletal sand shoals accumulated preferentially in former paleotopographic lows of 1–10 km in extent, and locally formed the foundation for reef development (Desrochers and James 1989).

METHODS

This study focuses on reefs from four sites within the Mingan Archipelago National Park Reserve: Île de la Fausse Passe, Île Nue de Mingan, Île du Fantôme, and Grande Pointe (Figs. 1, 3). At each locality, reef locations were waymarked using a hand-held Garmin GPS unit, which was held over the center of each reef (see associated data for reef locations). A tape measure was used to determine the thickness and diameter of reefs. Where a reef was elliptical in plan view, both the

long axis and short axis dimensions were measured, and the orientation of the long axis was measured using a compass.

Reef composition was quantified using point counting, following a procedure used by Kröger et al. (2017). A piece of thread, approximately 50 cm in length, with knots at 5 cm intervals, was laid across the rock surface, and the reef fossil or sedimentary matrix occurring at each knot point was recorded. This process was repeated until about 60 points had been counted within a reef core, or until it became difficult to locate the rock surface over which points had not already been counted. Because bryozoans and sponges are often identified using microscopic features, we used genus-level identification or form categories as categories for point counts. We also incorporated point count data published by Kröger et al. (2017), standardizing the categories used.

Point counts were collected only from the best-exposed and best-preserved reefs. At Île du Fantôme and Île de la Fausse Passe, which contain extensive reef exposures, we recorded the locations of all exposed reefs, subjectively estimated the proportions of reef-builders to classify reefs into qualitative categories (e.g., 'sponge-dominated', 'bryozoan-dominated', 'sponge-bryozoan'), and then point-counted representative reefs from the resulting qualitative categories. This allows for a spatial analysis of the distribution of reef types at these two sites. At Île Nue de Mingan and Grande Pointe, which have less extensive reef exposures, we omitted the mapping but otherwise followed the same procedure. The result is that while point counts do not comprehensively cover all exposed reefs at any of the four sites visited, we consider them to be representative of the variation in reef composition at and between sites.

The sedimentary context of the reefs was documented using field logs and sketches, providing an environmental and sequence stratigraphic context for reef development and for episodes of major reef growth. The intra-Mingan paleokarst was used as a marker horizon for measuring the stratigraphic height of reefs, where necessary and possible.

Data analysis was performed using R version 3.5.1 (R Core Team 2018). Point counts were used to evaluate the compositional heterogeneity of all reefs visited, by performing a complete-linkage cluster analysis based on the Bray-Curtis dissimilarity, an abundance-based pairwise measure of assemblage difference (Bray and Curtis 1957), which we calculated using the vegan package in R (Oksanen et al. 2018). A Bray-Curtis dissimilarity of 0 indicates that two sites contain an identical assemblage, while a dissimilarity of 1 indicates that they contain no shared compositional attributes. Because a large number of reefs (> 30) are exposed on Île du Fantôme and Île de la Fausse Passe, we also performed separate hierarchical cluster analyses of the point-counted compositions of reefs at these two localities, to evaluate reef heterogeneity at smaller spatial scales.

RESULTS

Compositional Cluster Analysis of All Reefs

The hierarchical cluster analysis of all reef core compositions (Online Supplemental File Tables 1–4) shows that reefs divide into two main compositional clusters (Fig. 4). Reefs from Grande Pointe and Île de la Fausse Passe are found in both clusters, while reefs at Île du Fantôme and Île Nue de Mingan are restricted to a single cluster. This indicates that reef compositions at Île Nue de Mingan and Île du Fantôme are more uniform than those at Grande Pointe and Île de la Fausse Passe, though reefs at Île du Fantôme also show considerable heterogeneity.

Descriptions of Reef Exposures

Grande Pointe.—At Grande Pointe, two stacked bioherms are exposed in a low (2 m) cliff beside a wave-cut platform (Fig. 5A). The bioherms are hosted within a bedded skeletal grainstone, and separated by a recessive weathering carbonate mudstone layer.

The lower bioherm is at least 5 m in diameter and 1 m thick, and is matrix-rich, with skeletal wackestone comprising 56% of its volume. The major skeletal components are tabulate corals, including loosely aggregated *in situ* heads of *Eofletcheria*, which range from a few centimeters to 30 cm across and comprise 37% of the bioherm core (Fig. 5B). *Eofletcheria* shows variable morphologies, forming both domical and columnar colonies (Fig. 5C). *Billingsaria* is also present

towards the top of the bioherm, though remains at low overall abundance (4%) (Fig. 5D). Encrusting, fenestrate, and ramose bryozoans are present, but making small volumetric contributions which are below detection in the point count. Encrusting bryozoans forming an open, chain-like pattern occur on *Billingsaria* sheets (Fig. 5E). At the bioherm margins, *Eofletcheria* and *Billingsaria* form alternating layers at centimeter scale, forming complexes up to 15 cm across (Fig. 5D). Small concentrations of disarticulated rhynchonellid brachiopods and cephalopods also occur at reef margins (Fig. 5F).

The overlying bioherm is ~ 3 m in diameter and is dominated by encrusting bryozoans, which comprise 55% of the bioherm volume and in places form bryolith-like textures described by Kröger et al. (2017) (Fig. 6A–6C). The wackestone matrix is much scarcer than in the underlying bioherm, comprising 14% of its volume. *Eofletcheria* is a much more minor component than in the lower bioherm, at 9%, and transported fragments are frequently encrusted by *Billingsaria* (9%) and bryozoans, which form layers centimeters thick (Fig. 6D). Sheets of *Billingsaria* and encrusting bryozoans (*Batostoma*?) often alternate, and bind lenses of grainstone (Fig. 6B). The resulting textures are reminiscent of bryoliths (Ernst et al. 2015), but the extent of transport remains ambiguous.

Île du Fantôme.—About 43 reefs are exposed in the Grande Pointe Member of the Mingan Formation on the southwest coastline of Île du Fantôme (Fig. 7). The reefs occur in an approximately 300 m wide belt to the south of an exposure of the intra-Mingan paleokarst unconformity between the Grande Pointe Member and the Perroquet Member. The intra-Mingan unconformity shows locally high relief (~ 20 m) (Figs. 7, 8A). The reefs occupied the northern side of a paleo-trough, with the shallowest water and rocky shoreline to the north around Anse à Michel, and the deepest water to the south, where the intra-Mingan unconformity proceeds below modern-day sea level.

Reefs at Île du Fantôme are predominantly bioherm complexes (e.g., Fig. 8B) though isolated bioherms also occur. The reef complexes are often aligned and individual non-circular reef cores are oriented with long axis in an approximately northeast-southwest direction, perpendicular to the trend of the reef band (Fig. 9) (Online Supplemental File Table 5). The median reef thickness is 1.1 m (n = 14, range = 0.5–2 m), and the median reef diameter is 6 m (n = 12, range = 2–15 m).

There is considerable compositional variation between bioherms, even when they occur within the same complex. The major metazoan reef components are lithistid sponges and encrusting bryozoans, making differing volumetric contributions between reefs. Reefs fall into two compositional clusters, though one cluster contains only a single reef, which is distinguished from the others by being particularly matrix-rich (Fig. 9) (point count data available in Online Supplemental File Table 2). The larger compositional cluster contains two subclusters; here, we discuss these separately as subcluster 1 and subcluster 2. A single example of a mud mound bioherm with stromatactis textures was also found at Île du Fantôme, which contained no visible skeletal frame-builders. This bioherm was not point counted, and so was excluded from the cluster analysis.

Bioherms in subclusters 1 and 2 contain approximately the same average proportion of wackestone matrix, but significantly different proportions of lithistid sponges and encrusting bryozoans based on Wilcoxon rank sum tests (Table 1). Subcluster 1 bioherms are richer in sponges, while subcluster 2 bioherms are richer in encrusting bryozoans. Compositional gradation between the subclusters mean that qualitative descriptions of ‘sponge-dominated’ and ‘bryozoan-sponge’ reefs do not consistently reflect membership of any cluster, though bryozoan-dominated bioherms are restricted to subcluster 2.

Bioherms in subcluster 1 have a reef core where lithistid sponges are the dominant metazoan component. Within reef cores, sponges show globular, conical, club-shaped, or cup-shaped morphologies, and often co-occur with patches of encrusting bryozoans. Where they occur, encrusting bryozoans are a volumetrically minor reef component (7%, n = 3, range = 2–16%) and

are commonly concentrated towards the bases and margins of the reef core, sometimes encrusting upon the sponges themselves (Fig. 8C, 8D).

In bryozoan-dominated bioherms, encrusting bryozoans form textures comparable with bryoliths described from both fossil and recent soft-sediment environments (Ernst et al. 2015). These structures may show diffuse boundaries and have a mudstone or wackestone matrix indistinguishable from the rest of the reef core (for examples of this texture from Grande Pointe, see Fig. 6A–6C). Lithistid sponges frequently occur in the margins of bryozoan-dominated bioherms or as intraclasts in flanking beds.

Other skeletal components also make a minor (< 5%) contribution to bioherms, including ramose bryozoans, pelmatozoan holdfasts, the foliaceous bryozoan *Phylloporina*, fenestrate bryozoans, and brachiopod and mollusk shells (Online Supplemental File Table 2). The top surfaces of bioherms commonly contain pelmatozoan roots at low abundances, indicating the presence of *in situ* pelmatozoans during bioherm accumulation (Fig. 8E). Transported skeletal material is abundant on reef flanks, including fragmentary lithistid sponges, echinoderm ossicles, and ramose bryozoans. Rarely, ramose bryozoans occur in life position on the top surfaces of reefs, forming thicket-like aggregations (Fig. 8F).

Sponge-dominated bioherms tend to occur in the southern end of the reef band, while bryozoan-dominated bioherms occur towards the north, suggesting a water depth control on reef composition (Fig. 9).

Île de la Fausse Passe.—At least 55 reefs are exposed within the Grande Pointe Member of the Mingan Formation on the east coast of Île de la Fausse Passe, forming a 410 m transect which deepens from north to south (Figs. 10, 11), as the intra-Mingan paleokarst surface descends towards sea level. The reefs have a median thickness of 1 m (n = 21, range = 0.4–2.5 m), and a median diameter of 2.1 m (n = 18, range = 1.5–8 m) (see Online Supplemental File Table 5).

The first generation of reefs nucleated on the intra-Mingan unconformity, but reef development continued throughout the marine transgression which characterized the Grande Pointe Member, nucleating on successive localized disconformities (Fig. 10). An overview of the east coast of Île de la Fausse Passe suggests two main episodes of reef development corresponding to the highstands within second-order sequences, which can be traced along the transect. Reefs are abundant towards the northern end of the transect, forming a reef band ~ 200 m wide, which progrades slightly towards the south (Fig. 10). At the southern edge of the reef band, beds grade into bedded wackestones with abundant *in situ* globular and bowl-shaped lithistid sponges, forming a deep-water ‘sponge meadow’ or sponge pavement, which also preserves oncolites and cephalopod shells (Fig. 12A, 12D).

Reefs at Île de la Fausse Passe comprise both isolated bioherms and bioherm complexes, with bioherm complexes progressively more dominant towards the southern end of the reef band (Fig. 12B, 12C). The reef matrix is a skeletal wackestone which contains fragmentary remains of trilobites, mollusks and brachiopods and ramose bryozoans. The dominant metazoan reef-builders are encrusting bryozoans, including *Ceramoporella* and *Batostoma*. The tabulate corals *Billingsaria* and *Eofletcheria* also occur in some reefs, and locally *Billingsaria* is the dominant metazoan frame-builder (Online Supplemental File Table 3). *Eofletcheria* is a less common reef contributor, and is generally less abundant than *Billingsaria*. Other minor reef components include mollusk fragments, *Girvanella* and lithistid sponges.

The compositional cluster analysis shows high dissimilarity in bioherm composition at Île de la Fausse Passe, with bioherms falling into two compositional clusters with a Bray-Curtis dissimilarity of ~ 0.8 (Fig. 11) (point count data are available in Online Supplemental File Table 3). The major compositional difference between bioherms in the two clusters is not the contribution of any key reef-builder, but the proportion of wackestone matrix; cluster 1 bioherms are, on average, more matrix-rich than cluster 2 bioherms (Table 2). Bioherms also contain minor taxa including lithistid

sponges, ramose bryozoans and brachiopods, which further contribute to this compositional heterogeneity.

Reefs where encrusting bryozoans are the dominant skeletal component are concentrated in the southern end of the exposure, but because these reefs typically occur ~ 1 m higher in the stratigraphy than those dominated by *Billingsaria*, the present-day north-south compositional gradient cannot be linked conclusively to paleo depth. Within bioherms, encrusting bryozoans typically dominate frame-building at lower levels of the reef core, while tabulate corals predominate on upper surfaces. Encrusting *Ceramoporella* and *Batostoma* commonly grow downwards at reef margins and on the undersides of *Billingsaria* sheets, occupying overhangs and suggesting growth in a sheltered, cryptic environment (figured in Kröger et al. 2017), though no evidence of a specialized cryptic fauna was found.

Île Nue de Mingan.—Île Nue de Mingan exposes a section through the Perroquet, Fantôme, and Grande Pointe members of the Mingan Formation, including a small exposure of the intra-Mingan unconformity (Fig. 13). Bioconstructions occur at two stratigraphic levels within the section: a biostrome about 2 m in thickness in the top half of the Perroquet Member, below the intra-Mingan unconformity, and a biohermal horizon in the Grande Pointe Member, approximately stratigraphically equivalent to the biohermal horizons at Île du Fantôme and Île de la Fausse Passe. The biostrome sits atop a scalloped erosional (karstic) grainstone surface (Fig. 14A, 14B), and contains abundant skeletal remains (Fig. 14C, 14E). The dominant metazoan components are lithistid sponges with branching, globular, cup-shaped or bowl-shaped morphologies, comprising a median 44% of the biostrome core (n = 3, range = 38–51%) (Fig. 14C, 14E). Most of the rest of the volume of the biostrome is skeletal grainstone matrix (mean 45%, n = 3, range = 31–54%). *Billingsaria* is also present, and is concentrated within the upper layers, contributing 7% of the biostrome volume in total (n = 3, range = 4–13%) (Fig. 14D). While the biostrome matrix contains abundant lithistid sponge, echinoderm and bryozoan fragments, *Billingsaria* sheets are seldom overturned, suggesting that they may be in life position (Fig. 14F). The Île Nue de Mingan biostrome can be classified as a heterogeneous autoparabiostrome, following Kershaw (1994), emphasizing the heterogeneity of constructor skeletons and the parautochthonous character of the deposition.

The bioherms have a different composition than the biostrome. Relatively few bioherms are exposed, and preservation only allows a comprehensive survey of bioherm constituents in a minority of cases. Two bioherms were point counted, and show considerable differences in composition. Both bioherms contain 41% skeletal wackestone matrix, and *Billingsaria* and the calcareous alga *Solenopora* are the major skeletal components (Fig. 12E, 12F). Lithistid sponges are present only in one bioherm (2%) (Fig. 12E) (point count data are available in Online Supplemental File Table 4). Other minor components include concentrations of cephalopods and trilobites in sedimentary pockets (e.g., similar to reefs of the Late Ordovician Vasalemma Formation of Estonia; Kröger et al. 2017), encrusting and ramose bryozoans, stromatoporoid fragments, and the bryozoan *Phylloporina*. Flanking beds are composed of grainstone.

DISCUSSION

This study assesses how Ordovician reef-building metazoans contributed habitat heterogeneity to their environments, by quantifying differences in reef composition at meter- to kilometer-scales using point counts made in the field. We begin with a discussion of the assumptions and limitations inherent in our approach, before discussing the implications of the results.

Because this study relates to fossil reefs, which have accumulated gradually and may not be precisely contemporaneous between islands, the data are somewhat time-averaged; however, we assume that since biohermal horizons occur within the same stratigraphic sequence, their facies can be considered to have been laterally equivalent (Walther's Law; Middleton 1973). The biostrome at Île Nue de Mingan is below the intra-Mingan unconformity, and so differences in composition between the biostrome and bioherms of the Grande Pointe Member do not represent spatial

heterogeneity; however, we include the biostrome in our analysis to compare biostrome and bioherm construction.

Our estimates of differences in the principal bioconstructors are likely to be underestimates, because we grouped encrusting bryozoans and lithistid sponges into single categories for point counting, and missed volumetrically minor taxa such as the tabulate corals *Lichenaria* and *Tetradium* (Desrochers and James 1989). The point counts reflect differences in the volumetric contribution and identity of reef-builders, but do not accurately reflect species-level taxonomic variation in the reef-building community, which can also influence reef-hosted diversity via species-specific trophic interactions (Messmer et al. 2011).

Finally, this study uses a combination of qualitative and quantitative (point count) observations in assessments of reef composition. Membership of a qualitative category can be a poor predictor of a bioherm's membership of a compositional cluster, where the volumetric contribution of wackestone matrix is a more important determinant of cluster membership (e.g., at Île de la Fausse Passe). However, it can be a helpful indicator where compositional clustering is based on the identity of the dominant reef-building metazoan (e.g., bryozoan-dominated reefs at Île du Fantôme). Therefore we use the point counts as our primary source of information on compositional differences between bioconstructions, but the qualitative data for evaluating spatial patterns in principal metazoan reef-builders.

Increasing Volumetric Contribution and Aggregation of Metazoan Reef-Builders

While skeletal metazoans with complex, robust, calcareous skeletons have inhabited reefs since at least the late Ediacaran (Wood et al. 2002; Wood and Penny 2018), they made a relatively small volumetric contribution to reefs worldwide. In lower Cambrian archaeocyath reefs of the Forteau Formation from Newfoundland and Labrador, Canada, archaeocyath skeletons constitute between 3.5 and 13.5% of the volume of the reef core (Pruss et al. 2012), while Toyonian archaeocyath reefs from Hubei Province, China, are up to 20% archaeocyath skeletal material (Adachi et al. 2015). Cambrian lithistid sponge reefs are similarly microbial dominated (e.g., Adachi et al. 2015). The reefs in this study, as at other Ordovician reef localities (e.g., Adachi et al. 2011), show a greater volumetric contribution from skeletal metazoans (up to ~ 50%), reflecting the increasing influence of metazoans on reef construction.

Notably, the most abundant reef-building skeletal metazoans of the Mingan reefs are not restricted to the reefs themselves, but also occur at lower density in the inter-reef deposits, and in the slightly older biostrome of the Perroquet Member. This is a pattern of occurrence which has long been noted in Paleozoic reef-builders such as stromatoporoids (Wood 1995; Kershaw et al. 2006). Hence, reef construction can be seen as an extreme on a continuum in spatial dispersal among sessile skeletal metazoans, from evenly dispersed to highly aggregated and from rare to abundant. Positive feedback cycles of niche construction and ecosystem engineering, as exemplified by the SLMs (sheet-like metazoans *sensu* Kröger et al. 2017) of the reefs of the Mingan Archipelago, may have facilitated spatial aggregation under a geohistorical regime of increasing abundance (e.g., Erwin 2008). The development of reef bands reflects the enhancement of seafloor relief by reef-building metazoans, both as a response to pre-existing seafloor relief and environmental conditions, but also a result of these positive feedbacks.

The development and expansion of skeletal metazoan reefs of the nearly time equivalent Chazy Group further to the west in Champlain Valley of New York and Quebec, which represent the initial climax of reefs dominated by bryozoans, corals, and stromatoporoids (e.g., Kapp 1975; Kröger et al. 2017), indicate that rapidly increasing abundances and a climax in reef formation during the late Middle Ordovician age were a regional phenomenon.

Controls on Reef Development in the Mingan Archipelago

The paleotopography of the intra-Mingan unconformity is a major control on the distribution of reefs within the Grande Pointe Member, constraining the distribution of grainstone facies at broad spatial scales (Desrochers 1985). The underlying topographic complexity generated by the intra-

Mingan unconformity appears to influence local-scale faunal composition. While the evidence for a depth-related zonation in reef composition at Île du Fantôme is somewhat equivocal, the distinction between coral-bryozoan reefs and the sponge pavement facies at Île de la Fausse Passe is extreme. Plausibly, depth-driven gradients in environmental conditions influenced the composition of benthic communities, even over local scales. The local-scale relief of the intra-Mingan unconformity contributed to habitat heterogeneity, both through generating spatial differences in hydrodynamic conditions, and by exerting control on reef development and reef-building communities.

Regionally, smaller scale sea-level fluctuations were also a control on reef development, mediated through the development of three calcarenite cycles within the Perroquet and Grande Pointe members of the Mingan Formation, which in places are capped with paleokarst surfaces which acted as a foundation for later reef and biostrome growth, as at Île Nue de Mingan (Desrochers and James 1988, 1989). Minor fluctuations in sea level are likely to have driven the formation of at least two generations of reef nucleation and growth at Île de la Fausse Passe.

Contribution of Skeletal Metazoans to Spatial Heterogeneity in a Middle Ordovician Seascape

Within-Reef Heterogeneity.—Local, centimeter-scale relief generated by the presence of skeletal organisms is a source of small-scale habitat heterogeneity in modern marine environments (Buhl-Mortensen et al. 2010; Kovalenko et al. 2012). Hemispherical *Eofletcheria* colonies and lithistid sponges would have generated up to tens of centimeters of local relief; these effects are common to bioherms, biostromes and inter-reef environments. In bioherms, sheet-like *Billingsaria* colonies could form overhangs sufficient to generate cryptic habitats. At Île de la Fausse Passe, the undersides of *Billingsaria* sheets at reef margins were colonized by encrusting bryozoans, now preserved with lateral or downward growth orientations (Kröger et al. 2017).

Between-Reef Heterogeneity.—In the Mingan Formation, differences in faunal composition between reefs at the same site, and between bioherms in the same complex, have been remarked upon before, as has the tendency for bioherms to be dominated by a single reef-building taxon, which may vary from one reef to another (e.g., Desrochers and James 1989). Because the architectures and mechanisms of reef formation of framework-building organisms vary between reefs within the Grande Pointe Member (e.g., Desrochers and James 1989), we can infer that reef-building metazoans generated heterogeneity in substrate type and local-scale conditions both within reefs and across the platform margin. This study is the first quantitative spatial analysis of these differences in reef assemblage composition in the Mingan Archipelago.

Reefs with distinct compositions in the Mingan Archipelago can be inferred to have provided different habitats. These compositional differences are pronounced, both between reefs in a single transect, and between exposures of the Grande Pointe Member, demonstrating that reef-building metazoans generated heterogeneity over 100 m scales and across the platform margin.

Compositional differences between reefs are likely to have resulted from a combination of environmental gradients, such as depth gradients, and ecological processes such as dispersal, which are not resolvable in our study but which impart some randomness in reef composition. An abundant, diverse reef-building community provides a mechanism for these processes to generate fine-scale habitat heterogeneity on the sea floor, in the form of compositional heterogeneity between reefs.

Taxonomic and morphological diversity in reef-building metazoans was not new in the Middle Ordovician; Cambrian reef-building communities were diverse (Kiessling 2005), and archaeocyaths showed a range of branching, massive and encrusting forms (Wood et al. 1992). However, the Middle Ordovician marks the widespread development of metazoan reefs combining reef-builder diversity and high volumetric contributions by skeletal metazoans.

CONCLUSIONS

Skeletal reef-building metazoans, including lithistid sponges, tabulate corals and bryozoans, generated seafloor heterogeneity at multiple spatial scales in the Middle Ordovician Grande Pointe Member of the Mingan Formation. The expansion of tabulate corals and bryozoans as reef-builders

alongside pre-existing lithistid sponge and algal assemblages allowed for high spatial heterogeneity in benthic communities at scales ranging from meters to kilometers, potentially increasing the capacity of shallow marine environments to host diverse communities.

The principal reef-building metazoans also occurred in inter-reef facies and in biostromes, exemplified by the biostrome in the upper Perroquet Member of the Mingan Formation. The construction of bands of bioherms reflects an enhancement of seafloor relief by metazoans, which may have in part been a response to local environmental conditions and underlying seafloor relief, but also an expression of positive feedbacks (ecosystem engineering and niche construction) which promoted spatial aggregation at a time when reef-building skeletal metazoans were increasingly abundant.

ACKNOWLEDGMENTS

We thank the staff of Parks Canada for processing our application to work in the Mingan Archipelago National Park Reserve, and are grateful to Danielle Shaienks for field assistance, Pierre St-Hilaire for transport to field localities, and Pierre Bertrand for drafting figures. We also thank two reviewers for their constructive comments. This work is part of the project *Ecological engineering as a biodiversity driver in deep time,* funded by the Academy of Finland. This paper is a contribution to the IGCP program 653 "The Onset of the Great Ordovician Biodiversification Event".

SUPPLEMENTAL MATERIAL

Data are available from the PALAIOS Data Archive: https://www.sepm.org/supplemental-materials.

REFERENCES

ADACHI, N., EZAKI, Y., AND LIU, J., 2011, Early Ordovician shift in reef construction from microbial to metazoan reefs: PALAIOS, v. 26, p. 106–114, doi: 10.2110/palo.2010.p10-097r.

ADACHI, N., EZAKI, Y., AND LIU, J., 2012, The oldest bryozoan reefs: a unique Early Ordovician skeletal framework construction: Lethaia, v. 45, p. 14–23, doi: 10.1111/j.1502-3931.2011.00268.x.

ADACHI, N., KOTANI, A., T., EZAKI, Y., AND LIU, J., 2015, Cambrian Series 3 lithistid sponge-microbial reefs in Shandong Province, North China: reef development after the disappearance of archaeocyaths: Lethaia, v. 48, p. 405–416, doi: 10.1111/let.12118.

ADACHI, N., LIU, J., AND EZAKI, Y., 2013, Early Ordovician reefs in South China (Chenjiahe section, Hubei Province): deciphering the early evolution of skeletal-dominated reefs: Facies v. 59, p. 451–466, doi: 10.1007/s10347-012-0308-2.

ALVAREZ-FILIP, L., DULVY, N.K., GILL, J.A., CÔTÉ, I.M., AND WATKINSON, A.R., 2011, Flattening of Caribbean coral reefs: region-wide declines in architectural complexity: Coral Reefs, v. 30, p. 1051–1060, doi: 10.1007/s00338-011-0795-6.

BOLTON, T.E. AND CUFFEY, R.J., 2005, Bryozoa of the Romaine and Mingan Formations (Lower and Middle Ordovician) of the Mingan Islands, Quebec, Canada, *in* H.I. Moyano, J.M. Cancino, and P.N. Wyse Jackson (eds.), Bryozoan Studies 2004, Taylor & Francis Group, London: p. 25–41.

BRAY, J.R. AND CURTIS, J.T., 1957, An ordination of the upland forest communities of southern Wisconsin: Ecological Monographs, v. 27, p. 325–349.

BUHL-MORTENSEN, L., VANREUSEL, A., GOODAY, A.J., LEVIN, L.A., PRIEDE, I.G., BUHL-MORTENSEN, P., GHEERARDYN, H., KING, N.J., AND RAES, M., 2010, Biological structures as a source of habitat heterogeneity and biodiversity on the deep ocean margins: Marine Ecology, v. 31, p. 21–50, doi: 10.1111/j.1439-0485.2010.00359.x.

DESROCHERS, A., 1985, The Lower and Middle Ordovician platform carbonates of the Mingan Islands, Quebec: stratigraphy, sedimentology, paleokarst, and limestone diagenesis: Unpublished Ph.D. thesis, Memorial University of Newfoundland, St. John's, 460 p.

DESROCHERS, A., BRENNAN-ALPERT, P., LAVOIE, D., AND CHI, G., 2012, Regional stratigraphic, depositional and diagenetic patterns from the interior of the St. Lawrence Platform: the Lower Ordovician Romaine Formation, western Anticosti Basin, Québec, *in* J.R. Derby, R.D. Fritz, S.A. Longacre, W.A. Morgan, and C.A. Stembach (eds.), The Great American Carbonate Bank: The Geology and Economic Resources of the Cambrian-Ordovician Sauk Megasequence of Laurentia: AAPG Memoir 98, p. 525–543.

DESROCHERS, A. AND JAMES, N.P., 1988, Early Paleozoic surface and subsurface paleokarst: Middle Ordovician carbonates, Mingan Islands, Québec, in Paleokarst: Springer, New York, NY, p. 183–210.

DESROCHERS, A. AND JAMES, N.P., 1989, Middle Ordovician (Chazyan) bioherms and biostromes of the Mingan Islands, Quebec, *in* H.H.J. Getdsetzer, N.P. James, and G.E. Tebbutt (eds.), Reefs, Canada and Adjacent Area: Canadian Society of Petroleum Geologists Memoir 13, p. 183–192.

DIX, G.R., NEHZA, O., AND OKON, I., 2013, Tectonostratigraphy of the Chazyan (late Middle–early Late Ordovician) mixed siliciclastic-carbonate platform, Quebec embayment: Journal of Sedimentary Research, v. 83, p. 451–474, doi: 10.2110/jsr.2013.39.

ERWIN, D.H., 2008, Macroevolution of ecosystem engineering, niche construction and diversity: Trends in Ecology and Evolution, v. 23, p. 304–310, doi: 10.1016/j.tree.2008.01.013.

ERNST, A., MUNNECKE, A., OSWALD, I. 2015, Exceptional bryozoan assemblage of a microbial-dominated reef from the early Wenlock of Gotland, Sweden: GFF, v. 137, p. 102–125, doi: 10.1080/11035897.2014.997543

JONES, C.G., LAWTON, J.H., AND SHACHAK, M., 1994, Organisms as ecosystem engineers: Oikos, v. 69, p. 373–386.

JONES, G.P., MCCORMICK, M.I., SRINIVASAN, M., AND EAGLE, J.V., 2004, Coral decline threatens fish biodiversity in marine reserves: Proceedings of the National Academy of Sciences of the United States of America, v. 101, p. 8251–8253.

KAPP, U.S., 1975, Paleoecology of Middle Ordovician stromatoporoid mounds in Vermont: v. 8, p. 195–207.

KERSHAW, S., 1994, Classification and geological significance of biostromes: Facies, v. 31, p. 81–92.

KERSHAW, S., WOOD, R., GUO, L., KERSHAW, S., WOOD, R., AND GUO, L.I., 2006, Stromatoporoid response to muddy substrates in Silurian limestones: GFF, v. 128, p. 131–138, doi: 10.1080/11035890601282131.

KIESSLING, W., 2005, Long-term relationships between ecological stability and biodiversity in Phanerozoic reefs: Nature, v. 433, p. 410–413, doi: 10.1029/2002JB001866.

KIESSLING, W., SIMPSON, C., AND FOOTE, M., 2010, Reefs as cradles of evolution and sources of biodiversity in the Phanerozoic: Science, v. 327, p. 196–198, doi: 10.1126/science.1182241.

KOVALENKO, K.E., THOMAZ, S.M., AND WARFE, D.M., 2012, Habitat complexity: approaches and future directions: Hydrobiologia, v. 685, p. 1–17, doi: 10.1007/s10750-011-0974-z.

KRÖGER, B., DESROCHERS, A., AND ERNST, A., 2017, The reengineering of reef habitats during the Great Ordovician Biodiversification Event: PALAIOS, v. 32, p. 584–599.

LEE, J.H. AND RIDING, R., 2018, Marine oxygenation, lithistid sponges, and the early history of Paleozoic skeletal reefs: Earth-Science Reviews, v. 181, p. 98–121, doi: 10.1016/j.earscirev.2018.04.003.

LI, Q., LI, Y.U.E., AND KIESSLING, W., 2017, The oldest labechiid stromatoporoids from intraskeletal crypts in lithistid sponge—*Calathium* reefs: Lethaia, v. 50, p. 140–148, doi: 10.1111/let.12182.

LINDSKOG, A., COSTA, M.M., RASMUSSEN, C.M.O., CONNELLY, J.N., AND ERIKSSON, M.E., 2017, Revised Ordovician timescale reveals no link between asteroid breakup and biodiversification: Nature Communications, v. 8, p. 14066.

McLaughlin, P.I., Emsbo, P., Desrochers, A., Bancroft, A.M., Brett, C., Riva, J., Premo, W., Neymard, L., Achab, A., Asselin, E., and Emmons, M., 2016, Refining two kilometers of Ordovician chronostratigraphy beneath Anticosti Island using integrated chemostratigraphy: Canadian Journal of Earth Sciences, v. 53, p. 865–74, doi:10.1139/cjes-2015-0242.

Messmer, V., Jones, G.P., Munday, P.L., Holbrook, S.J., Schmitt, R.J., and Brooks, A.J., 2011, Habitat biodiversity as a determinant of fish community structure on coral reefs: Ecology, v. 92, p. 2285–2298.

Middleton, G.V., 1973, Johannes Walther's law of the correlation of facies: Geological Society of America Bulletin, v. 84, p. 979–988.

Normore, L.S., Zhen, Y.Y., Dent, L.M., Crowley, J.L., Percival, I.G., and Wingate, M.T.D., 2018, Early Ordovician CA-IDTIMS U–Pb zircon dating and conodont biostratigraphy, Canning Basin, Western Australia: Australian Journal of Earth Sciences, v. 65, p. 61–73.

Oksanen, J., Blanchet, F.G., Friendly, M., Kindt, R., Legendre, P., McGlinn, D., Minchin, P.R., O'hara, R.B., Simpson, G.L., Solymos, P., Stevens, M.H.M., Szoecs, E., and Wagner, H., 2018, vegan: Community Ecology Package: R package version 2.5-2, https://CRAN.R-project.org/package=vegan.

Pratt, B.R. and James, N.P., 1982, Cryptalgal-metazoan bioherms of early Ordovician age in the St George Group, western Newfoundland: Sedimentology, v. 29, p. 543–569, doi: 10.1111/j.1365-3091.1982.tb01733.x.

Pruss, S.B., Clemente, H., and Laflamme, M., 2012, Early (Series 2) Cambrian archaeocyathan reefs of southern Labrador as a locus for skeletal carbonate production: Lethaia, v. 45, p. 401–410, doi: 10.1111/j.1502-3931.2011.00299.x.

R Core Team, 2018, R: A language and environment for statistical computing: http://www.r-project.org/.

Rigby, J.K. and Desrochers, A., 1995, Lower and Middle Ordovician lithistid demosponges from the Mingan Islands, Gulf of St. Lawrence, Quebec, Canada: Journal of Paleontology, v. 41, p. 1–35.

Roberts, C.M. and Ormond, R.F.G., 1987, Habitat complexity and coral reef fish diversity and abundance on Red Sea fringing reefs: Marine Ecology-Progress Series, v. 41, p. 1–8.

Rocha, L.A., Robertson, D.R., Roman, J., and Bowen, B.W., 2005, Ecological speciation in tropical reef fishes: Proceedings of the Royal Society B, Biological Sciences, v. 272, p. 573–579.

Rowland, S.M. and Shapiro, R.S., 2002, Reef patterns and environmental influences in the Cambrian and earliest Ordovician, *in* Kiessling, E.K. Flügel, and J. Golonka (eds.), Phanerozoic Reef Patterns: SEPM Special Publication, v. 72, p. 95-128.

Stigall, A.L., Edwards, C.T., Freeman, R.L., and Rasmussen, C.M.Ø., 2019, Coordinated biotic and abiotic change during the Great Ordovician Biodiversification Event: Darriwilian assembly of early Paleozoic building blocks: Palaeogeography, Palaeoclimatology, Palaeoecology, v. 530, p. 249–270, doi: 10.1016/j.palaeo.2019.05.034.

Webby, B.D., 2002, Patterns of Ordovician reef development, *in* W. Kiessling, E.K. Flügel, and J. Golonka (eds.), Phanerozoic Reef Patterns: SEPM Special Publication, v. 72, p. 129–179.

Wood, R. and Penny, A., 2018, Substrate growth dynamics and biomineralization of an Ediacaran encrusting poriferan: Proceedings of the Royal Society B: Biological Sciences, v. 285, p. 20171938. doi: 10.1098/rspb.2017.1938.

Wood, R.A., 1995, The changing biology of reef-building: PALAIOS, v. 10, p. 517–529, doi: 10.2307/3515091.

Wood, R.A., Grotzinger, J.P., and Dickson, J.A.D., 2002, Proterozoic modular biomineralized metazoan from the Nama Group, Namibia: Science, v. 296, p. 2383–2386, doi: 10.1126/science.1071599.

WOOD, R.A., ZHURAVLEV, A.YU, AND DEBRENNE, F., 1992, Functional biology and ecology of Archaeocyatha: PALAIOS, v. 7, p. 131–156.
Received 11 February 2020; accepted 18 July 2020.

FIGURE CAPTIONS

FIG. 1.—Geological map and geographic context map of the Mingan Archipelago. Geological map redrawn from Desrochers and James (1989). Localities visited for this study are labelled with their names.

FIG. 2.—Stratigraphic scheme, using Lindskog et al. (2017) for absolute dates for the biozones, with Floian zones adjusted according to Normore et al. (2018).

FIG. 3.—West-east cross section through the Mingan Archipelago, showing the paleotopography of the intra-Mingan unconformity (vertical scale exaggerated). Localities visited for this study are labelled with their names. Figure redrawn from Desrochers and James (1988).

FIG. 4.—Complete-linkage cluster analysis of the compositions of all point-counted reefs in the Mingan Archipelago, using the Bray-Curtis dissimilarity.

FIG. 5.—Features of the lower bioherm at Grande Pointe. **A**) Overview of upper and lower bioherms. Measuring stick is 1 m long; bioherms are outlined in white. Brightness enhanced by 20%. **B**) Hemispherical *Eofletcheria* colonies in the lower bioherm (white arrows = *Eofletcheria* colonies). Contrast enhanced by 20%. **C**) Columnar *Eofletcheria* colony. **D**) *Billingsaria* encrusting on a core of *Eofletcheria*, forming multiple dense layers. Encrusting bryozoans also form thinner layers in the surrounding area. **E**) Chain-like encrusting bryozoans preserved on the surface of a *Billingsaria* colony, showing characteristic surface texture. *Eofletcheria* is also visible, underlying the *Billingsaria*. **F**) Pocket of micrite at reef margin, containing cephalopod shells and other skeletal debris. Abbreviations: Bil = *Billingsaria*; Bry = encrusting bryozoans; Ceph = Cephalopod; Eo = *Eofletcheria*.

FIG. 6.—Features of the upper bioherm at Grande Pointe. **A**) Repeated layers of encrusting bryozoans forming a characteristic SLM fabric (labelled SLM, and outlined in dotted white lines). **B**) Encrusting bryozoans and ?*Billingsaria* forming convoluted sheets among bedded wackestones and grainstones. **C**) Alternating layers of encrusting bryozoans and *Billingsaria* forming a complex. **D**) *Billingsaria* encrusting a small core of transported *Eofletcheria*. Abbreviations: Bil = *Billingsaria*; Bry = encrusting bryozoan; Eo = *Eofletcheria*; SLM = sheet-like metazoan.

FIG. 7.—Section through the coastline at Île du Fantôme, showing the stratigraphy and distribution of reefs.

FIG. 8.—Reefs,reef components and the Intra-Mingan unconformity at Île du Fantôme. **A**) Intra-Mingan unconformity at Anse au Michel, showing complex local relief. Geological hammer is ~ 0.3 m long. **B**) Bioherm complex, weathered out to form a monolith. This weathering allows 3D examination of reef textures and components. **C**) A globular lithistid sponge encrusted by bryozoans in a sponge-bryozoan reef. **D**) Sponge from C in context, showing rubbly reef texture. **E**) Pelmatozoan holdfasts preserved *in situ* in the top surface of a sponge-bearing reef. **F**) Ramose bryozoan thicket, preserved *in situ.* Abbreviations: Bry = encrusting bryozoan; Pel = pelmatozoan holdfast.

FIG. 9.—Map of reef locations at Île du Fantôme, and complete-linkage hierarchical cluster analysis using the Bray-Curtis dissimilarity as a distance measure.

FIG. 10.—Reconstruction of section at Île de la Fausse Passe, showing locations of reefs.

FIG. 11.—Map showing locations of reefs at Île de la Fausse Passe, and complete-linkage hierarchical cluster analysis of reef compositions using the Bray-Curtis dissimilarity as a distance measure.

FIG. 12.—Bioherms in the Grande Pointe Member at Île de la Fausse Passe and Île Nue de Mingan. **A**) Relatively distal, sponge pavement facies at Île de la Fausse Passe, with *in situ* lithistid sponges (examples highlighted with white arrows). **B**) Section through bioherm complex at Île de la Fausse Passe, showing the geometry in relation to surrounding beds. Bioherm complex outlined in white.

C) Coastal exposure at Île de la Fausse Passe, showing multiple reefs. **D**) Oncolites in the sponge pavement facies (examples highlighted with white arrows). **E**) Bioherm at Île Nue de Mingan showing *Solenopora* and lithistid sponges in a bioherm core. **F**) *Billingsaria* and *Solenopora* forming a framework texture within a bioherm at Île Nue de Mingan. Abbreviations: Bil = *Billingsaria*; S = *Solenopora*; L = Lithistid.

FIG. 13.—Stratigraphic section at Île Nue de Mingan, showing context for the reefs and biostrome and some sedimentological features.

FIG. 14.—Biostrome horizon in the Perroquet Member of the Mingan Formation at Île Nue de Mingan. **A**) Outcrop overview of the biostrome horizon, with cross-bedding visible in the underlying strata of the Perroquet Member. The base of the biostrome is highlighted with a dotted white line. **B**) Scalloped karst surface underlying the biostrome. **C**) Rudstone textures within the biostrome including lithistid sponge, *Billingsaria* and encrusting bryozoans. **D**) *Billingsaria* preserved upright in the biostrome. **E**) Globular lithistid sponges in the top surface of the biostrome. **F**) *Billingsaria* laminae preserved upright in the top surface of the biostrome. Abbreviations: Bil = *Billingsaria*; Bry = encrusting bryozoan; S = lithistid sponge.

TABLE CAPTIONS

TABLE 1.—Differences in composition between bioherms in subclusters 1 and 2 at Île du Fantôme.

TABLE 2.—Differences in composition between bioherms in clusters 1 and 2 at Île de la Fausse Passe.

Ekuanitshit

Longue-Pointe

Havre-Saint-Pierre

50°25' N

Île Nue de Mingan

Île du Fantôme

La Grande Pointe

Île de la Fausse Passe

Mingan Formation

Romaine Formation

Precambrian

Town

① Biostrome

② Bioherm

③ Bioherm complex

0 10

Km

64°00' W

63°50' W

50°00' N

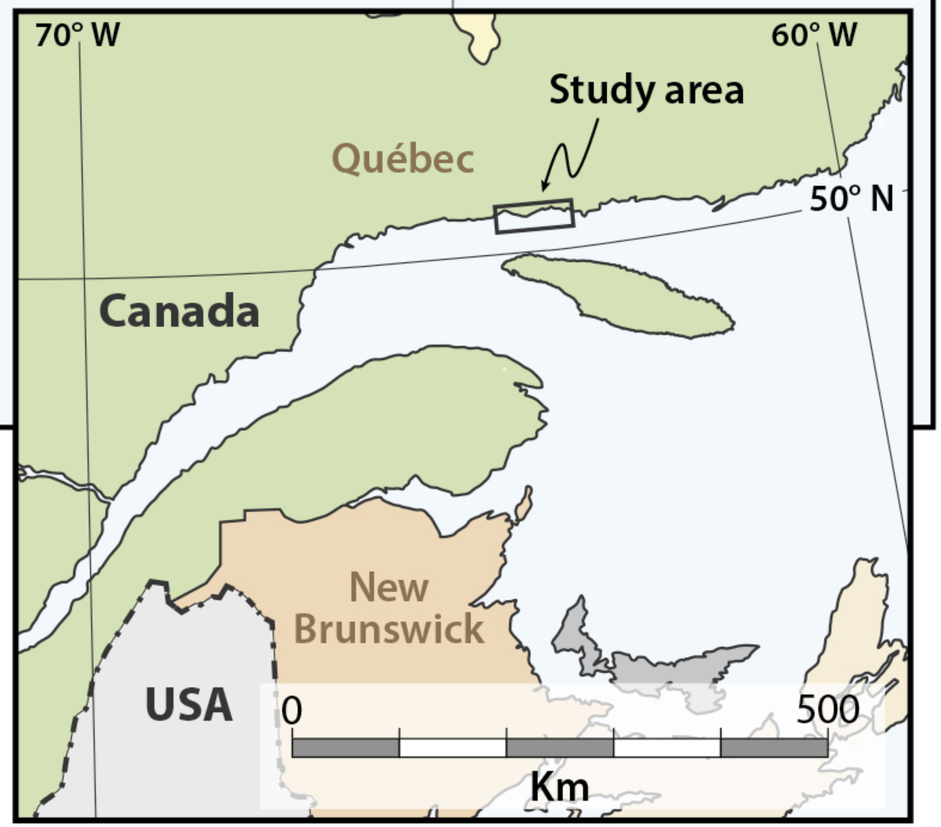

mya	Stage	Stage slice	Regional stage	Lithostratigraphy Mingan Islands		
	Darriwilian	Dw 3	Chazyan	Mingan Fm	Grande Pointe Mbr	① ② ③
					Fantôme Mbr	①
					Perroquet Mbr	
					Corbeau Mbr	
		Dw 2	No regional stage recognized			
		Dw 1				
467.3						
	Dapingian	Dp 2				
		Dp 1	Rangerian		Grande Île Mbr	
470.0						
	Floian	Fl 3	Blackhillsian	Romaine Fm	Ste-Geneviève Mbr	
		Fl 2				
		Fl 1	Tulean		Sauvage Mbr	
477.7						
	Tremadocian	Tr 3	Stairsian			
		Tr 2				
		Tr 1	Skullrockian			
485.4						

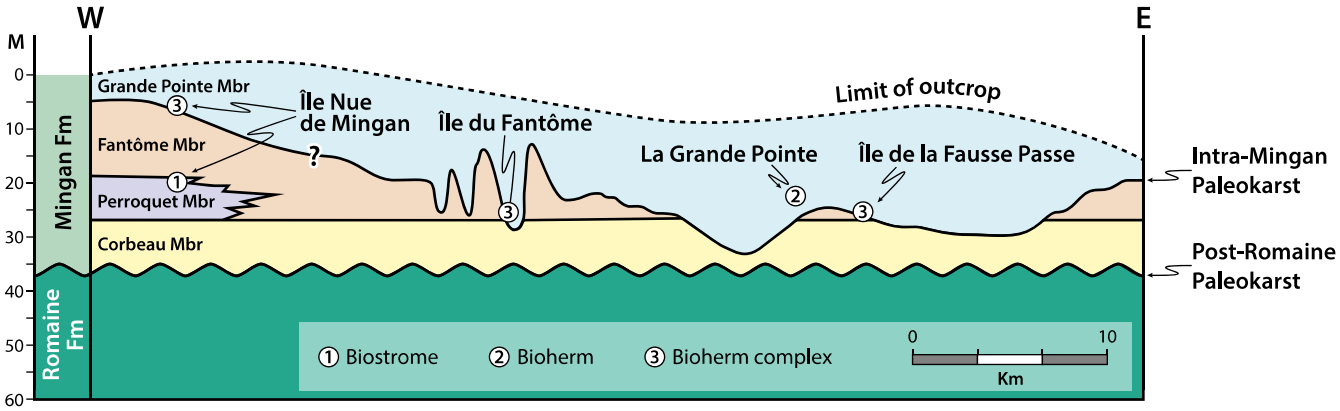
W
E
M
0
10
20
30
40
50
60
Mingan Fm
Romaine Fm
Grande Pointe Mbr
Fantôme Mbr
Perroquet Mbr
Corbeau Mbr
Île Nue de Mingan
?
Île du Fantôme
La Grande Pointe
Île de la Fausse Passe
Limit of outcrop
Intra-Mingan Paleokarst
Post-Romaine Paleokarst
① Biostrome
② Bioherm
③ Bioherm complex
0
10
Km

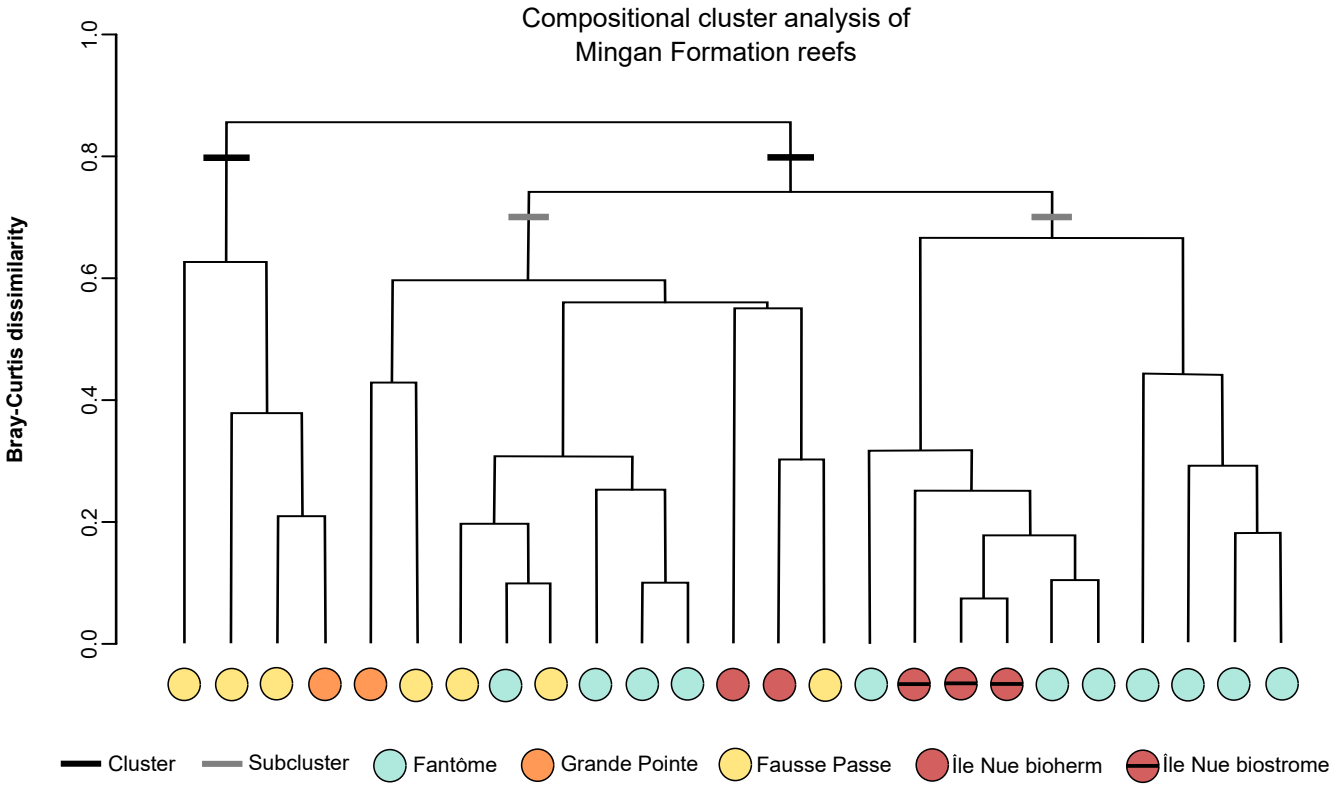
Compositional cluster analysis of
Mingan Formation reefs
Bray-Curtis dissimilarity
0.0
0.2
0.4
0.6
0.8
1.0
Cluster
Subcluster
Fantôme
Grande Pointe
Fausse Passe
Île Nue bioherm
Île Nue biostrome

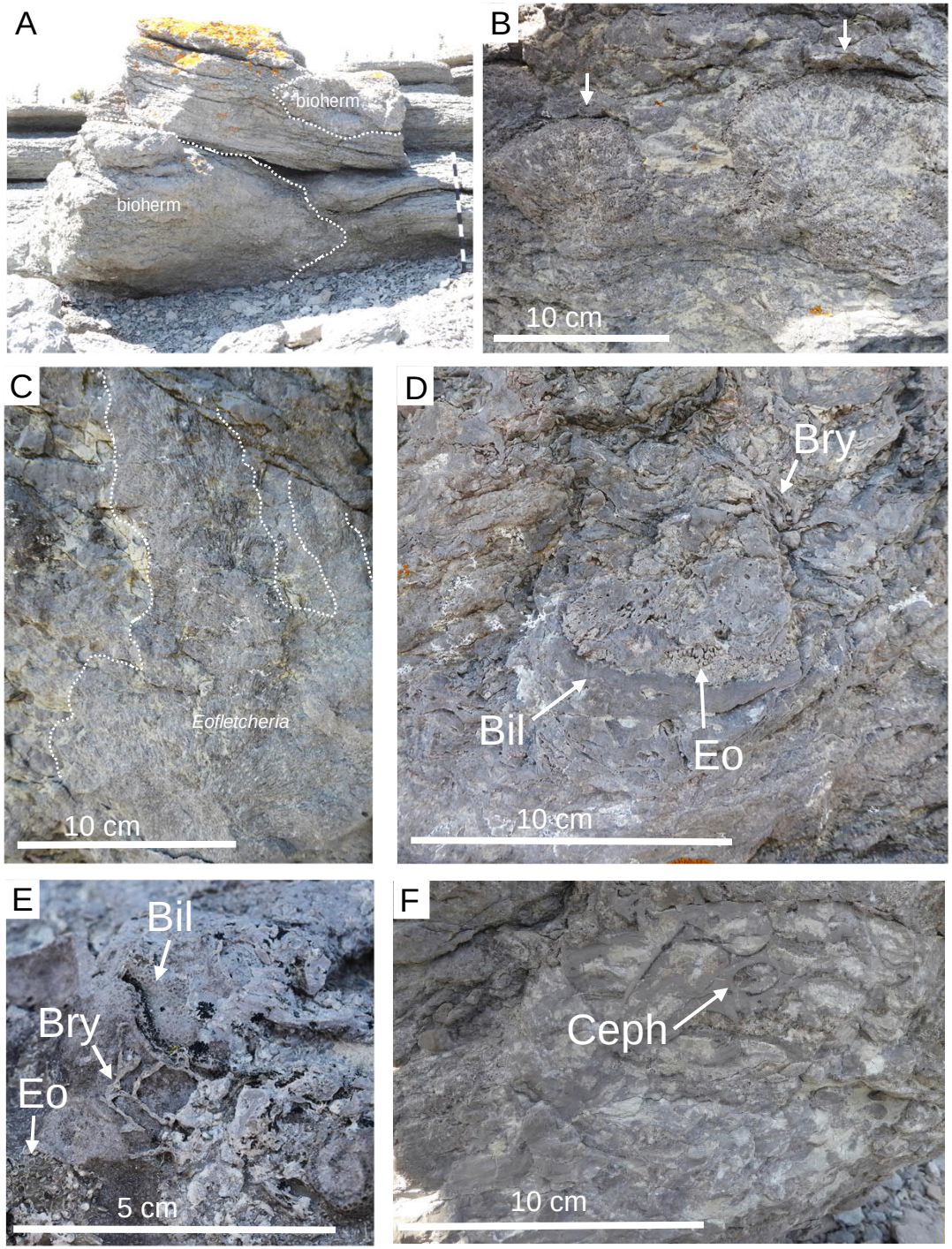
A
bioherm
bioherm
B
10 cm
C
Eofletcheria
10 cm
D
Bry
Bil
Eo
10 cm
E
Bil
Bry
Eo
5 cm
F
Ceph
10 cm

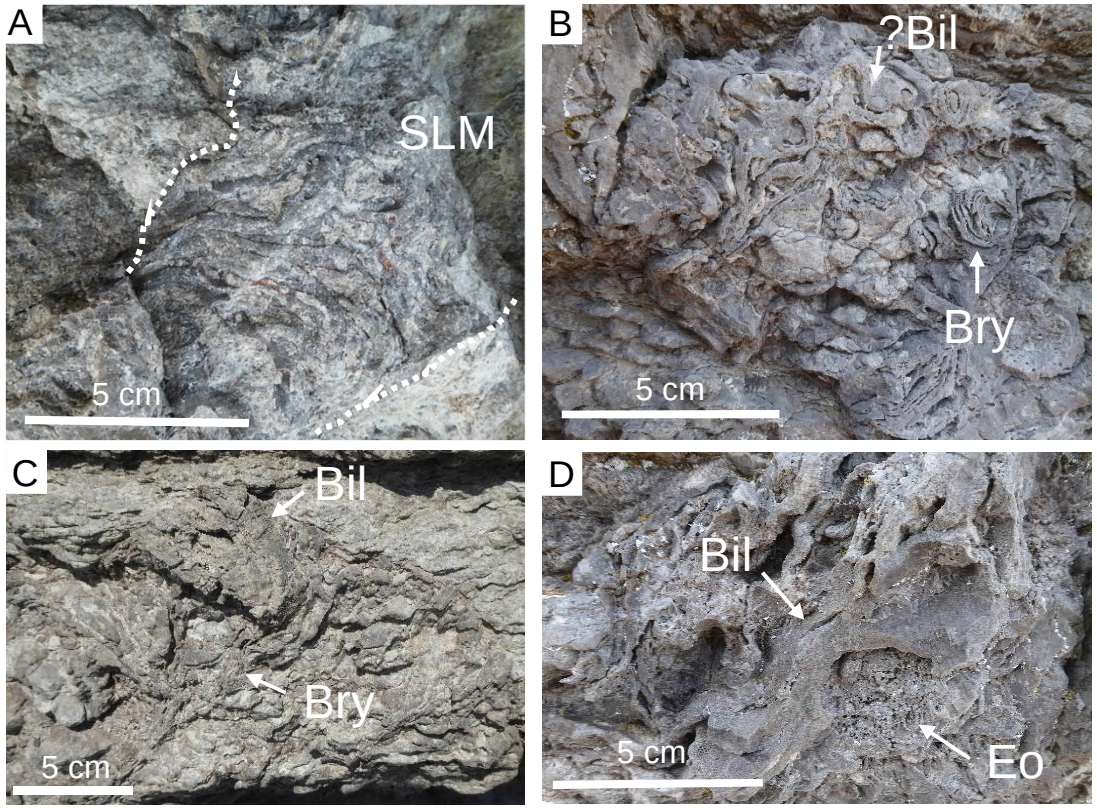
A
SLM
5 cm
B
?Bil
Bry
5 cm
C
Bil
Bry
5 cm
D
Bil
5 cm
Eo

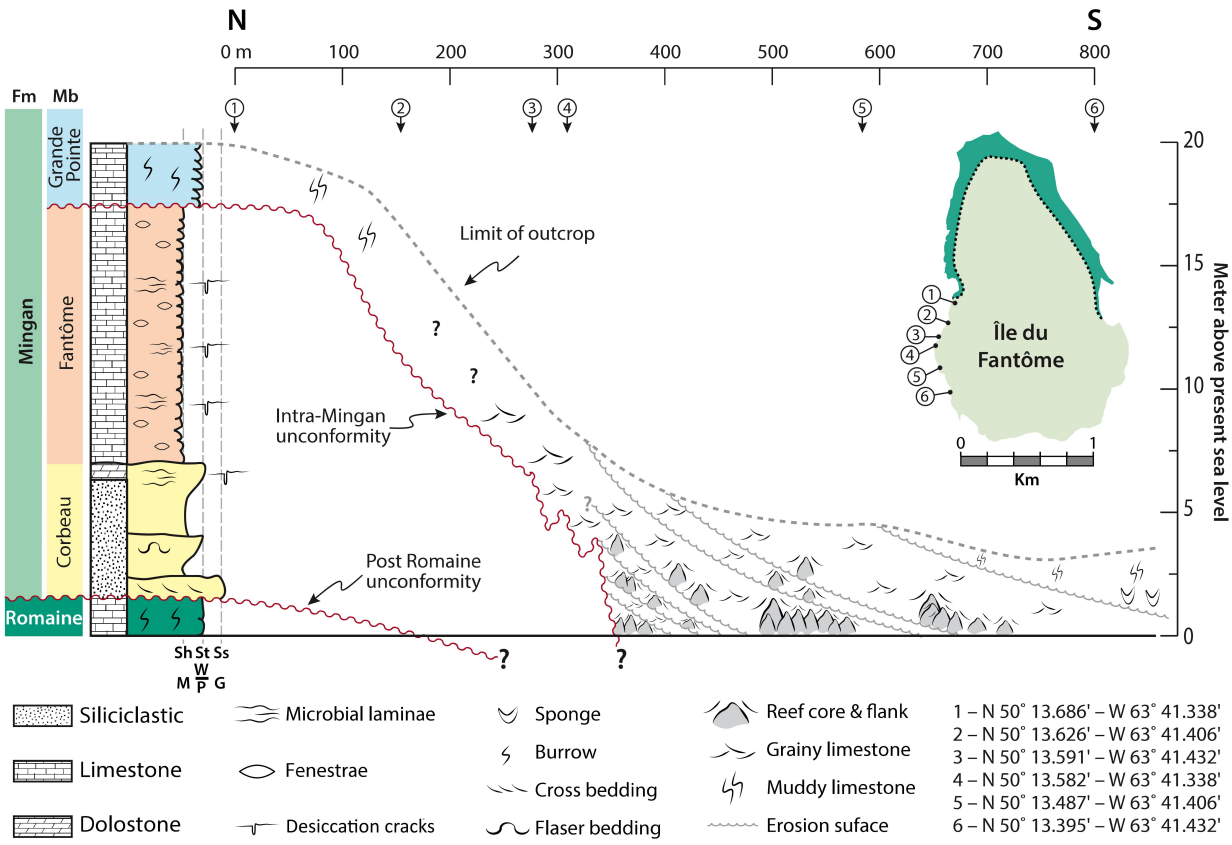
N
S
0 m
100
200
300
400
500
600
700
800
Fm
Mb
Mingan
Grande Pointe
Fantôme
Corbeau
Romaine
Limit of outcrop
Intra-Mingan unconformity
Post Romaine unconformity
Île du Fantôme
0
1
Km
20
15
10
5
0
Meter above present sea level
Sh St Ss
M W/P G
Siliciclastic
Limestone
Dolostone
Microbial laminae
Fenestrae
Desiccation cracks
Sponge
Burrow
Cross bedding
Flaser bedding
Reef core & flank
Grainy limestone
Muddy limestone
Erosion suface
1 – N 50° 13.686' – W 63° 41.338'
2 – N 50° 13.626' – W 63° 41.406'
3 – N 50° 13.591' – W 63° 41.432'
4 – N 50° 13.582' – W 63° 41.338'
5 – N 50° 13.487' – W 63° 41.406'
6 – N 50° 13.395' – W 63° 41.432'

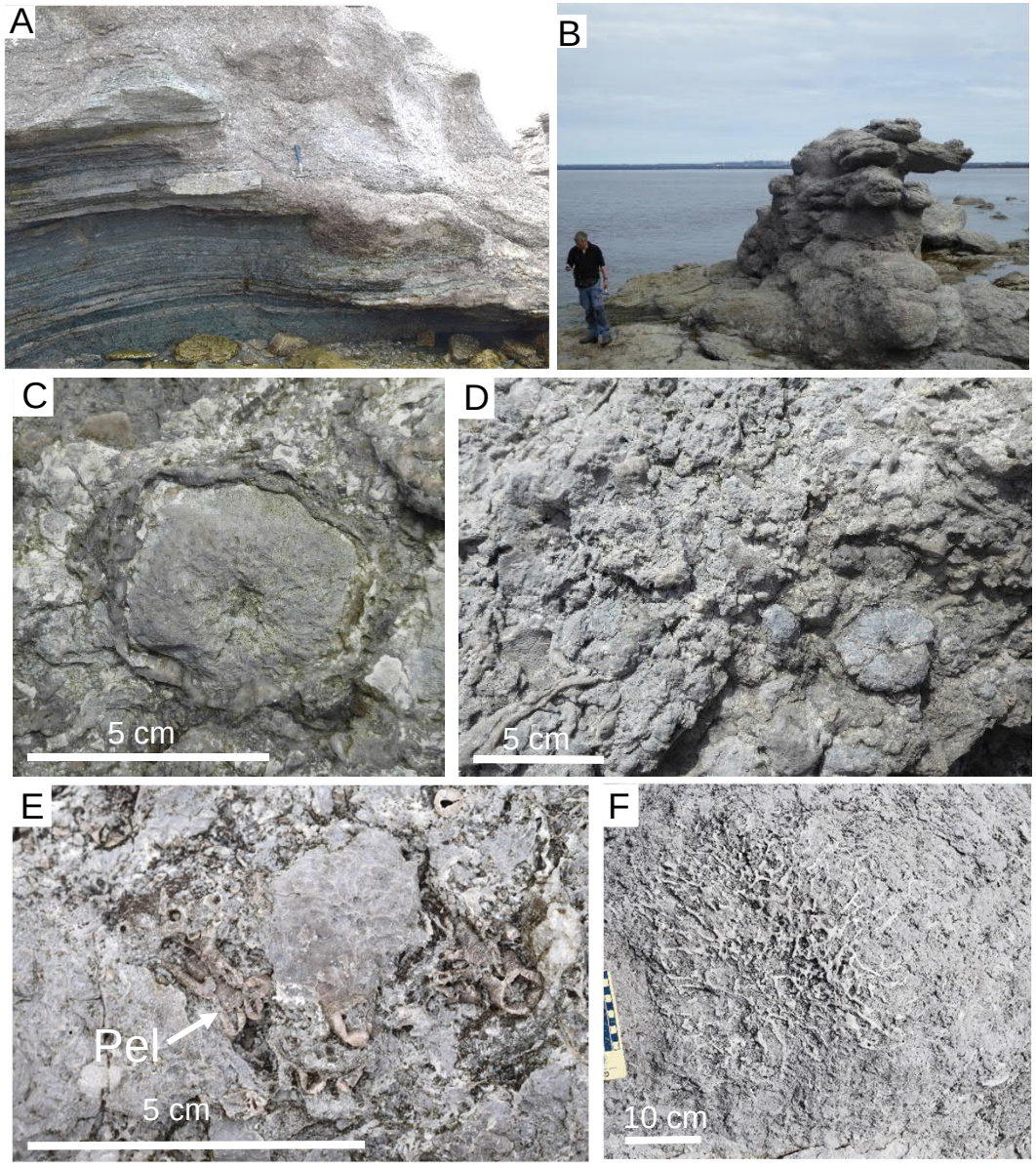
A
B
C
5 cm
D
5 cm
E
Pel
5 cm
F
10 cm

Hierarchical cluster analysis of reefs at Île du Fantôme

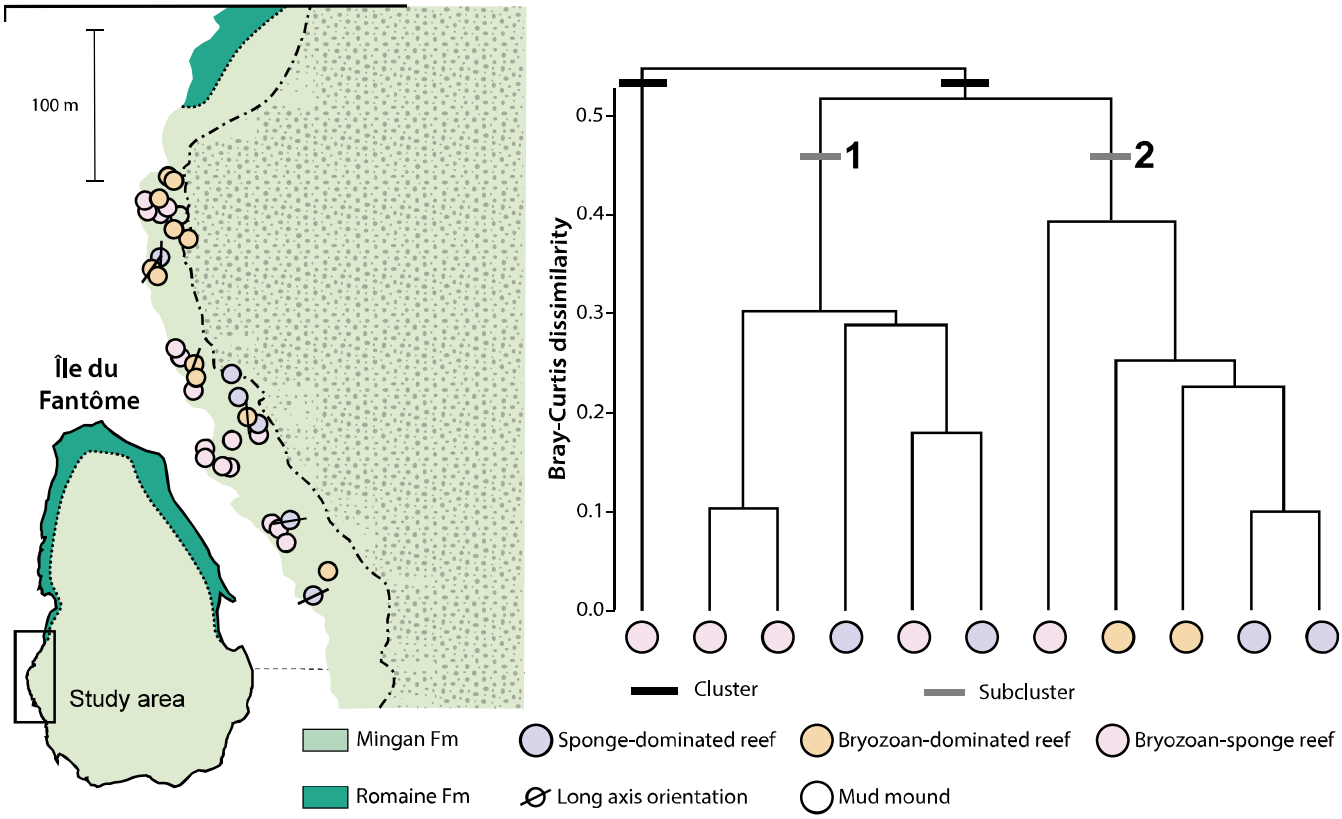

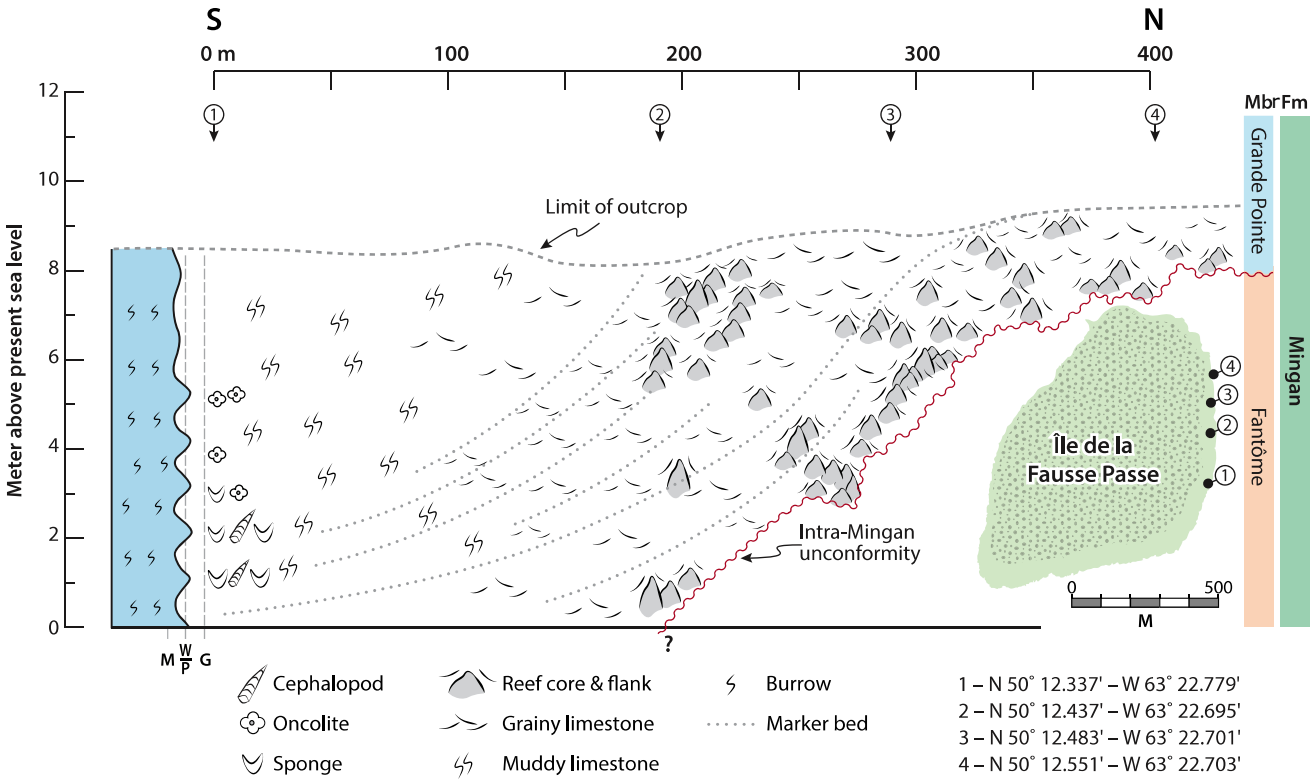
S
N
0 m
100
200
300
400
Meter above present sea level
12
10
8
6
4
2
0
Limit of outcrop
Mbr
Fm
Grande Pointe
Fantôme
Mingan
Île de la
Fausse Passe
Intra-Mingan
unconformity
0
500
M
M
W
P
G
?
Cephalopod
Oncolite
Sponge
Reef core & flank
Grainy limestone
Muddy limestone
Burrow
Marker bed
1 – N 50° 12.337' – W 63° 22.779'
2 – N 50° 12.437' – W 63° 22.695'
3 – N 50° 12.483' – W 63° 22.701'
4 – N 50° 12.551' – W 63° 22.703'

Hierarchical cluster analysis of reefs at Île de la Fausse Passe

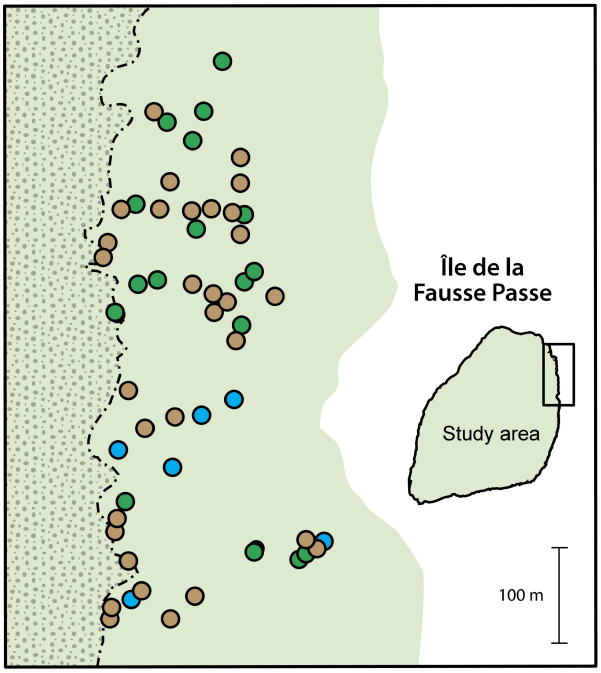

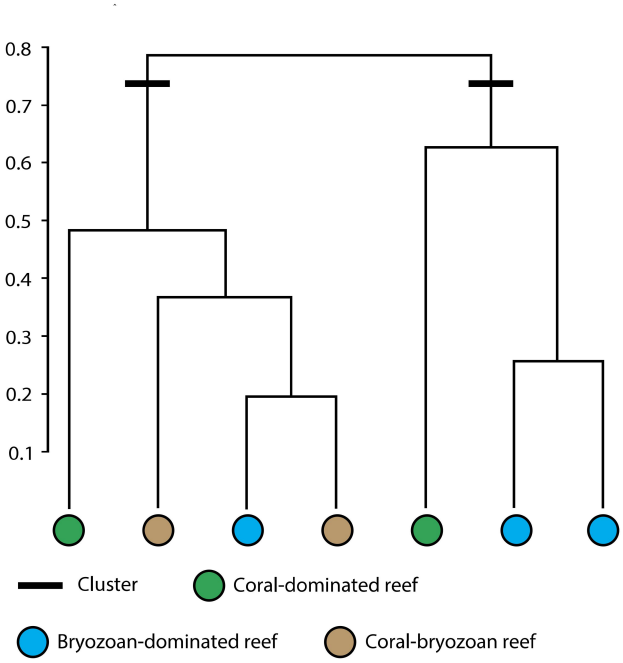

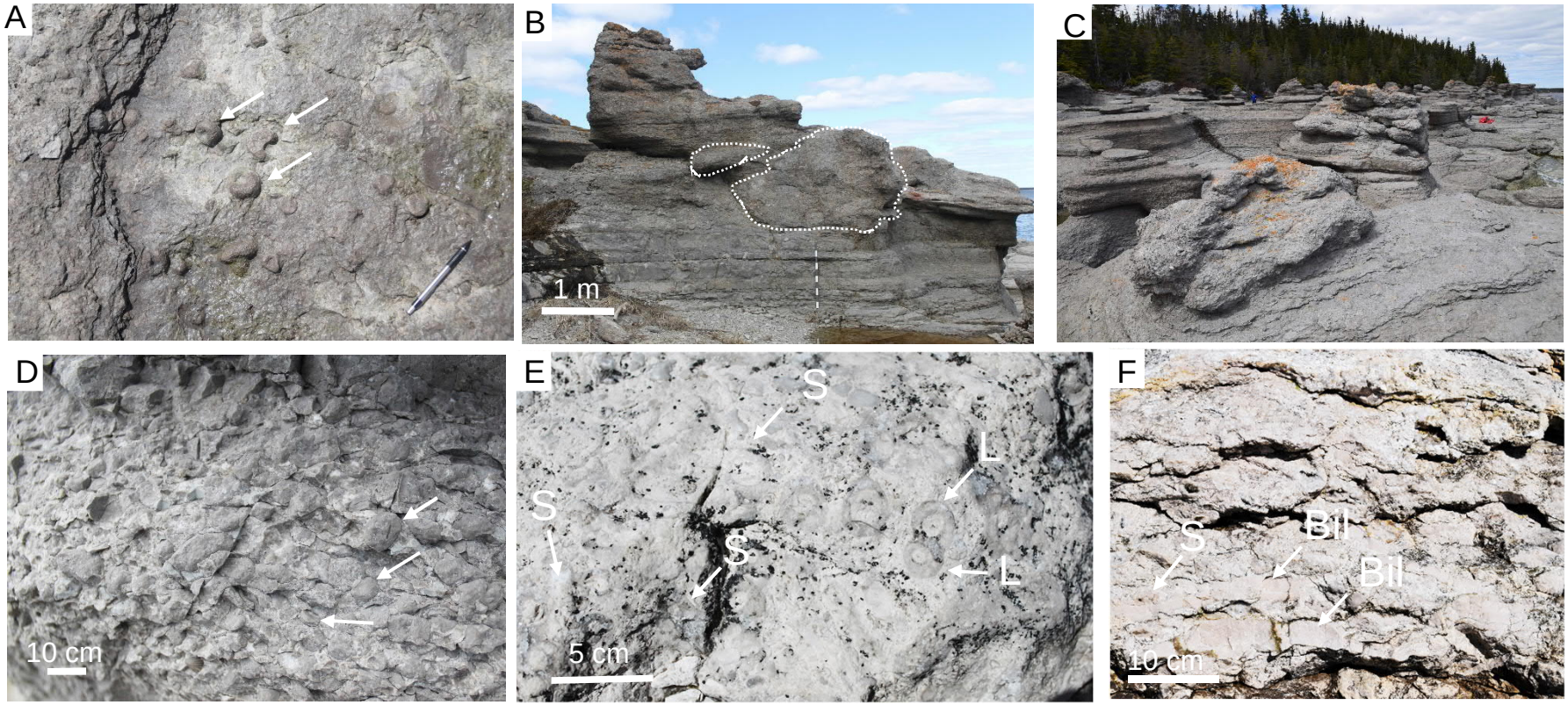
A
B
1 m
C
D
10 cm
E
S
L
S
S
L
5 cm
F
S
Bil
Bil
10 cm

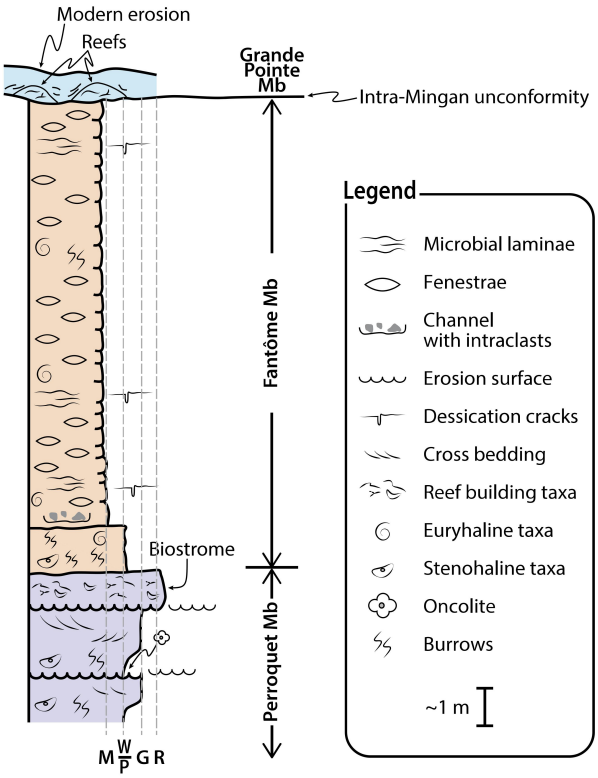
Modern erosion
Reefs
Grande Pointe Mb
Intra-Mingan unconformity
Fantôme Mb
Perroquet Mb
Biostrome
M W/P G R
Legend
Microbial laminae
Fenestrae
Channel with intraclasts
Erosion surface
Dessication cracks
Cross bedding
Reef building taxa
Euryhaline taxa
Stenohaline taxa
Oncolite
Burrows
~1 m

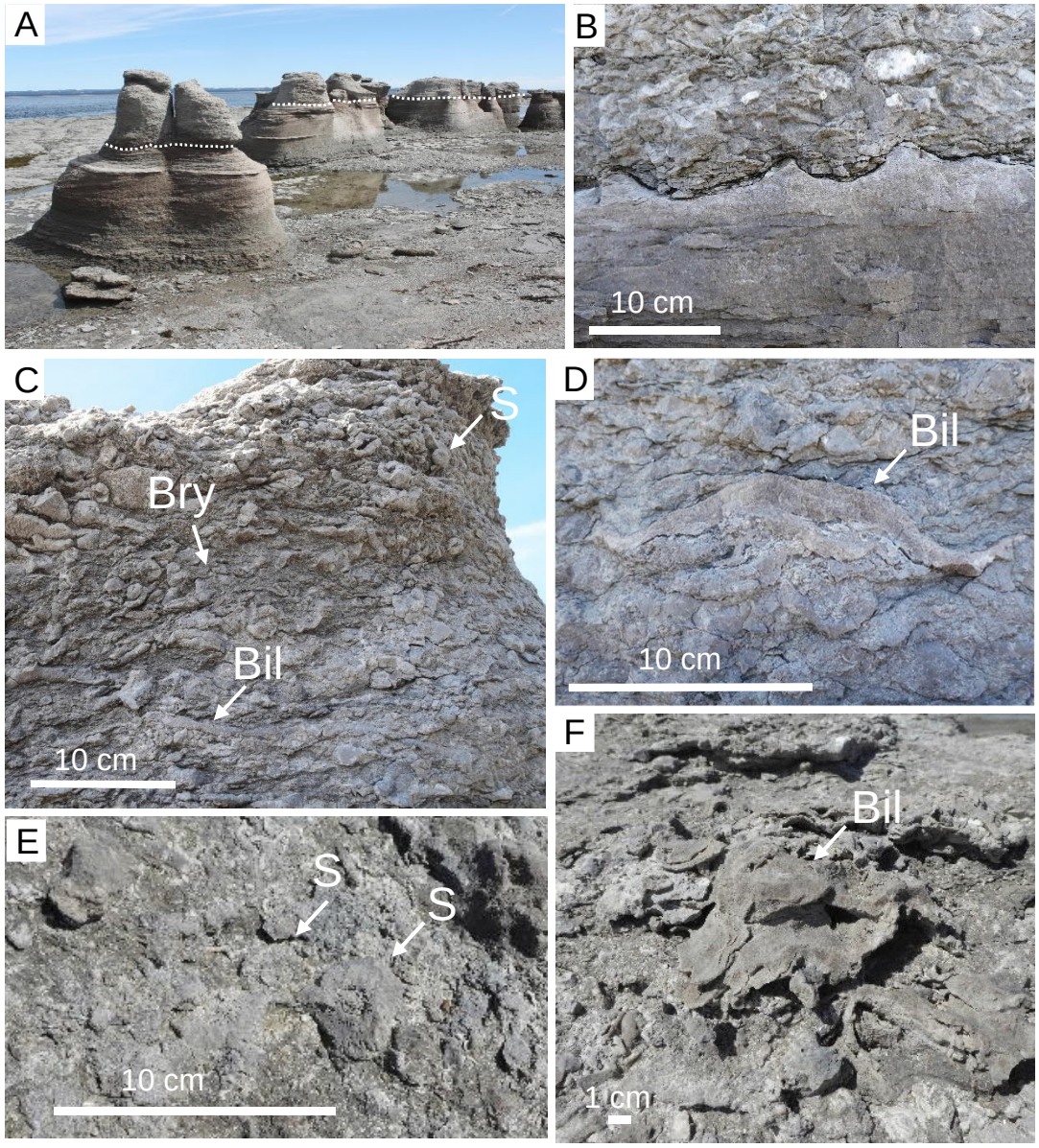
A
B
10 cm
C
S
Bry
Bil
10 cm
D
Bil
10 cm
E
S
S
10 cm
F
Bil
1 cm